ELSEVIER

Materials Science and Engineering A 425 (2006) 1–6

MATERIALS SCIENCE & ENGINEERING A

www.elsevier.com/locate/msea

Mechanism of mechanical property enhancement in nitrogen and titanium implanted 321 stainless steel

Ming Xu [a], Liuhe Li [b], Youming Liu [a,c], Xun Cai [a,*], Qiulong Chen [a], Paul K. Chu [c]

[a] *School of Materials Science and Engineering, Shanghai Jiao Tong University, Shanghai 200030, China*
[b] *702 Department, Mechanical Engineering School of Beijing University of Aeronautic and Astronautic, Beijing 100083, China*
[c] *Department of Physics and Materials Science, City University of Hong Kong, Kowloon, Hong Kong*

Received 26 July 2005; received in revised form 2 March 2006; accepted 9 March 2006

Abstract

Ion implantation is a well-known method to modify surface mechanical properties. The improvement of the mechanical properties can usually be attributed to the formation of new strengthening phases, solution strengthening, dislocation strengthening, or grain refinement. However, in many cases, the roles of individual factors are not clear. In this study, we implanted nitrogen and titanium into 321 stainless steel samples to investigate the enhancement mechanism of the mechanical properties. Nano-indentation experiments were conducted to measure the hardness under various loadings. The N and Ti implanted 321 stainless steel samples were found to behave differently in the hardness (GPa) versus depth (nm) diagram. The effects of the radiation damage, solution strengthening, and dispersion strengthening phase were analyzed. Characterization of the modified layers was performed using techniques such as Auger electron spectroscopy (AES) and grazing incidence X-ray diffraction (GIXRD). Transmission electron microscopy (TEM) and X-ray diffraction were also applied to reveal the structure of the untreated 321 stainless steel.

PACS: 52.77; 81.65L; 46.70; 46.55

Keywords: Ion implantation; Nano-indentation hardness; 321 stainless steel; Strengthening mechanism

1. Introduction

Ion implantation can be used to modify the surface properties of materials such as the mechanical characteristics and improve the tribological behavior of the materials. Unlike other thermodynamically limited processes such as diffusion, the quantity of the implanted elements is not confined by solubility and phase diagrams. In principle, any element can be implanted into any material substrates and there is no obvious interface between the modified layer and substrate.

A number of previous studies have dealt with the influence of ion implantation on the mechanical properties of thin layers, particularly the hardness [1–4]. Ion implantation produces micro-structural changes which may strengthen the surface. The types of changes resulting from ion implantation include the creation of defects, phase transformations, and formation of intermetallics [5]. In particular, extensive research work has been done on the strengthening of steels using nitrogen or titanium ion implantation. In addition to the synergistic effects of substitutional and interstitial species, the increase in hardness is mainly attributed to the fine dispersion of hard second-phase precipitates [6–9]. In the case of nitrogen ion implantation, micro-alloying is achieved resulting in implantation-induced defects, supersaturated solid solutions, and precipitation of intermetallic compounds [10–15]. The depth distribution of the nitrides and formation of a solid nitrogen solution γ_N are also responsible for the mechanical property enhancement [16–18]. In the case of titanium ion implantation, the analysis has been focused on the formation of TiC and phase transformations [19,20]. For example, martensite transformation occurs during implantation into H13 consequently altering the surface hardness [9]. Moreover, an amorphous surface layer is usually found and it contributes to the improvement of the hardness as well [21]. It has also been suggested that the implantation temperature and ion energy may contribute to the final effects of hardness improvement [22,23]. Nano-hardness testing is one of the most widely used methods

* Corresponding author. Tel.: +86 21 62932087; fax: +86 21 62932587.
E-mail address: xcai@sjtu.edu.cn (X. Cai).

0921-5093/$ – see front matter © 2006 Elsevier B.V. All rights reserved.
doi:10.1016/j.msea.2006.03.040

to measure the surface mechanical properties of thin layers. This technique measures the penetration under different indentation loads to obtain an indentation curve. From these measured data, the mechanical properties such as hardness and elastic modulus can be evaluated [24–27].

Although previous investigations have generated valuable insight into the mechanical property enhancement mechanism, there have been relatively few studies on the effects of deformation such as the ones induced by radiation damage or strengthening phases caused by ion implantation on hardness. In this study, it is found that the Ti and N implanted layers in 321 stainless steels exhibit different hardness versus depth relationships. The phenomenon may be due to different hardening mechanisms. An analytical solution is difficult to obtain based on the indentation data alone since indentation is a highly nonlinear technique in which large deformation, large strain, material nonlinearity, and contacts are involved, and consequently, Auger electron spectroscopy (AES) and small angle X-ray diffraction (GIXRD) are also employed to investigate the strengthening mechanism.

2. Experimental details

In this study, 321 stainless steels were chosen as the substrates because of their exclusive austenitic structure. Such a simple structure can reduce the interference on the hardness measurement due to nonuniform substrate composition. The chemical composition (wt%) is Fe, 70.1; C, 0.11; Si, 0.90; Cr, 18.2; Ni, 9.40; Ti, 0.64; S, 0.06; and P, 0.03. The dimensions of samples were 20 mm × 20 mm × 3 mm. All of them were austenitized at 1500 K for 1 h to achieve a solid solution state and then highly polished. Prior to ion implantation, the samples were cleaned in acetone, dehydrated ethanol, and distilled water sequentially in an ultrasonic bath. Nitrogen ion implantation was conducted using a Kaufman ion source with 99.999% high purity nitrogen. Titanium implantation was conducted utilizing a pulsed metal vapor vacuum arc (MEVVA) ion source. The purity of the titanium cathode was 99.8%. During the implantation processes, the samples were positioned on a water cooled sample stage. The ion implantation parameters are listed in Table 1.

Auger electron spectroscopy was employed to determine the depth profiles of the implanted layer with Ar^+ sputtering at an etching speed of 6 nm/min. Because of the thin modified layer, grazing incidence X-ray diffraction at an incident angle 1° was used to identify the various phases of the implanted samples and the scanning range was from 25° to 90°. Moreover, micro-structural observations of untreated samples were carried out by transmission electron microscopy (TEM) and X-ray diffraction.

The hardness measurements were performed by using a nano-indenter with a CSM three-sided pyramidal diamond (Berkovich) indenter. The hardness values were calculated based on the method used by Oliver and Pharr [28,29]. Six maximum loads of 0.1, 0.50, 1.00, 1.5, 2.50, and 4 mN were adopted. Three or Four indents were applied for each load for statistical purpose.

Table 1
Ion implantation parameters

Implanted element	Nitrogen	Titanium
Base pressure (Pa)	1.5×10^{-3}	1.5×10^{-3}
Acceleration voltage (kV)	70	50
Acceleration current (mA)	10.8	8.3
Process duration (s)	5400	7200
Ion current density (μA/cm^2)	15	12
Implantation dose (cm^2)	5×10^{17}	5×10^{17}

3. Results and discussion

Fig. 1(a) depicts the titanium depth profile in the 321 stainless steel. The Ti profile displays a Gaussian like distribution with the peak atomic fraction reaching 36% at a depth of approximately 33 nm. According to TRIM simulation, the peak depth should be about 20 nm. The deeper distribution is a result of the multiple charge states of Ti emitted from the MEVVA source. Using multi-peak Gaussian fitting (Fig. 1(b)) and TRIM simulation of the ion ranges with various energies (Table 2), the average ion charge state of Ti is determined to be 1.7. That is to say, if the accelerating voltage is 50 kV, the mean Ti implantation energy is ∼85 keV. The total "implanted" depth or thickness of the modified layer is about 140 nm. As shown in Fig. 1(c), the as-implanted nitrogen profile remains roughly symmetrical. During 70 kV implantation, the sample temperature is about 250–300 °C. Slight broadening and decreased peak concentration (∼21%) at the depth of ∼77 nm are observed. Nitrogen accumulation (∼10%) starts at the surface and extends into the substrate, implying some degree of diffusion.

The grazing incidence X-ray diffraction results displayed in Fig. 2 disclose the micro-structures of the two implanted samples. For comparison, XRD and TEM were also performed on the unimplanted substrate to confirm the original structure. The electron diffraction pattern of the unimplanted sample is indexed as γ-Fe [0 1 1] of the face-centered-cubic structure (Fig. 3). The diffraction peaks of γ-[Fe, C, Ni] can be found either in the substrate and the two implanted samples, suggesting that Ni, Ti, and Cr exist on the lattice sites of the main phase [γ-Fe] whereas C is present as interstitial atoms. Except for the Fe_2TiO_4 phase caused by oxidation in the examination, no evidence of transformation is found in the unimplanted specimen. In addition to γ-[Fe, C, Ni], new families of peaks are observed from the implanted samples.

As to the Ti implanted sample, it is observed that the Ni_3Ti and $Ti_{5.73}C_{3.72}$ phases are newly formed after implantation. According to Grabowski and Kants' work on thermal conduction of metal implantation [30], the temperature rise during metal source

Table 2
Ion range of Ti implanted into 321 stainless steel with various energies

	50 keV	55 keV	60 keV	65 keV	70 keV	80 keV	90 keV
R_P (Å)	202	221	239	257	275	311	348

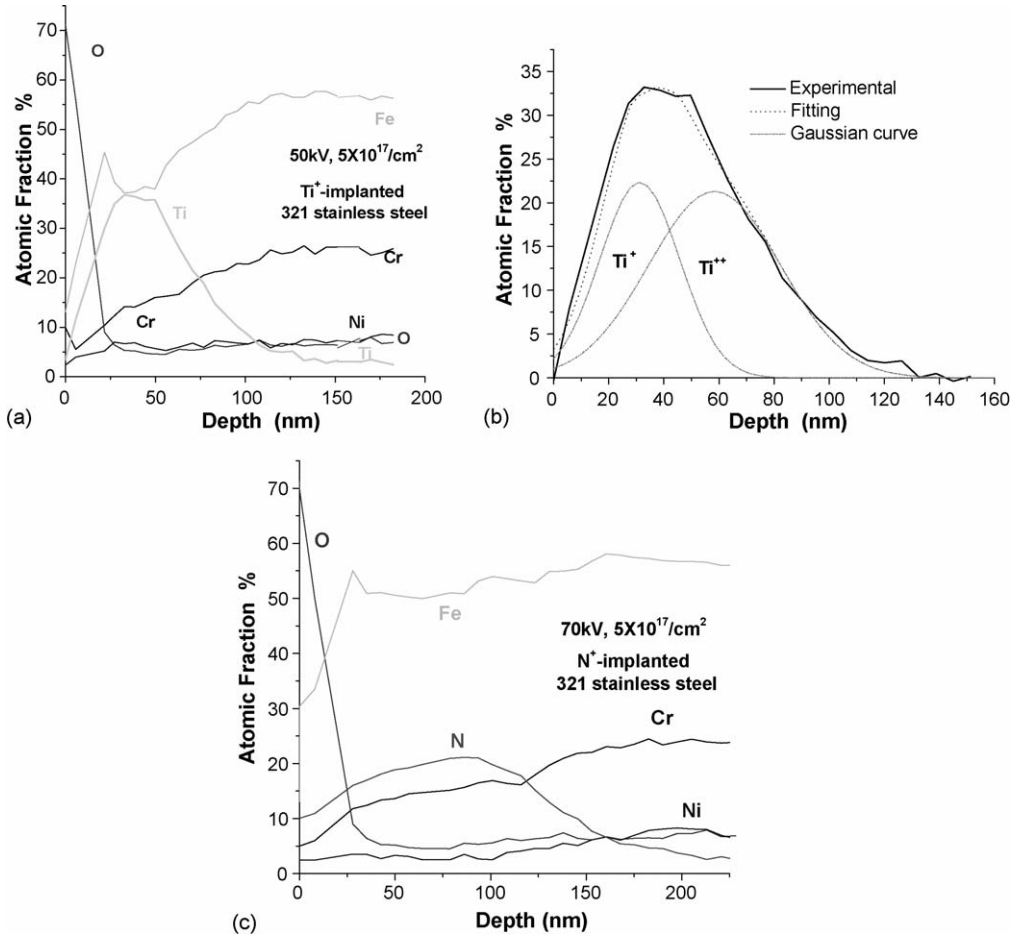

Fig. 1. Elemental depth profiles obtained by sputtering Auger electron spectroscopy: (a) titanium implanted sample, (b) multi-peaks Gaussian fitting for Ti profile curve, and (c) nitrogen implanted sample.

ion implantation can be given as follows:

$$T_s - T_0 = \frac{Jl}{K} \tag{1}$$

and

$$J = \frac{\text{ion energy} \times \text{ion current}}{\text{sample area}}\ (\text{W/cm}^2), \tag{2}$$

where T_0 is the initial temperature, T_S the surface temperature of the sample, J the incidence power, l the thickness of sample, and K is the coefficient of thermal conduction. The K value of 304 stainless steels is 0.16 W/(cm K). Thus, the temperature rise ($T_S - T_0$) of the Ti implanted sample can be estimated to be ~355 °C. As suggested by Zhang et al. [31,32], the dispersion strengthening effects are dominated if the implantation temperature T is selected as $0.25T_m < T < 0.6\ T_m$, where T_m is the melting point of the sample. The T_m of 321 stainless steels is approximately 1370–1400 °C. Therefore, the Ti-implantation temperature is beneficial to the formation and growth of dispersion strengthening phases such as Ni_3Ti and $Ti_{5.73}C_{3.72}$.

As shown by the equally strong peak besides the peak of γ-[Fe, C, Ni], a large quantity of expanded austenite γ_N is detected after nitrogen ion implantation. Free nitrogen atoms diffuse to defects in the crystalline lattice or octahedral and tetrahedral sites of the fcc austenitic structure to form γ_N solid solution, which generates compressive residual stresses [33,34]. In addition, small quantities of ferrous nitride (FeN) and chromium nitride (CrN and Cr_2N) are observed from the weak peaks. The formation of nitride is contributed to locking dislocations due to plastic deformation.

Fig. 4 compares the hardness profiles for two implanted samples calculated using the method of Oliver and Pharr and implantation elements distribution measured by AES. Although the mechanical properties are determined by the complex interactions between the implanted layer and bulk substrate, the hardness versus depth curve more or less corresponds to the implantation profile. However, the hardness of the Ti implanted layer is highest on the surface whereas that of the nitrogen implanted sample appears at a deeper position around R_p zone.

The AES results indicate that the nitrogen depth distribution deviates somewhat from an "implant-like" Gaussian profile. It has been reported that the nitrogen distribution in the austenitic stainless steels is controlled by thermal diffusion in the temperature range from 150 to 500 °C [35]. By taking in account the X-ray diffraction patterns, it is proposed that the nitrogen depth distribution shown here is determined predominately by one of these three factors: ballistic mixing effect, chemical effect, and thermal diffusion. Adopting the LSS theory as well as surface

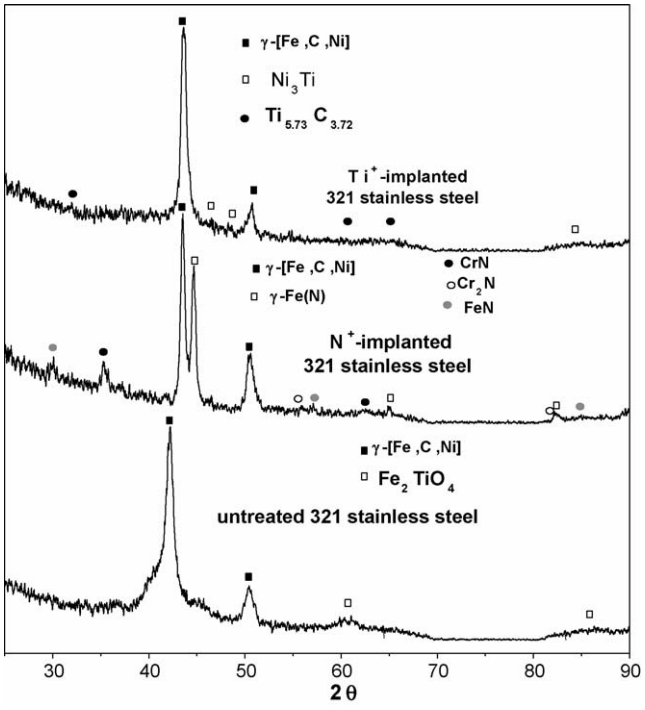

Fig. 2. Comparison between GIXRD patterns obtained from the nitrogen implanted sample and titanium implanted sample with XRD patterns from the unimplanted sample.

spattering effect and N thermal diffusion, the nitrogen distribution can be expressed as [35]:

$$C_{\mathrm{N}(x)} = \frac{n_0}{2Y}\left[\mathrm{erf}\frac{x - R_\mathrm{p} + S(\phi)}{\sqrt{2}\sqrt{\Delta R_\mathrm{p}^2 + 4Dt}} - \mathrm{erf}\frac{x - R_\mathrm{p}}{\sqrt{2}\sqrt{\Delta R_\mathrm{p}^2 + 4Dt}}\right], \tag{3}$$

where $C_{\mathrm{N}(x)}$ is the nitrogen atomic concentration at a depth x from the surface, n_0 the atomic density of substrate (cm^{-3}), Y

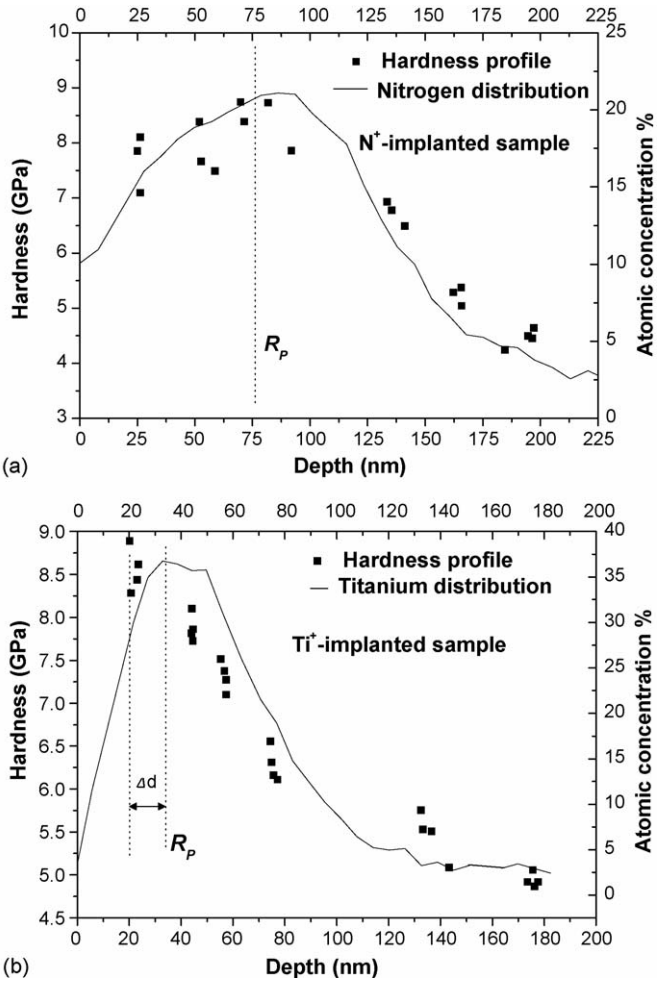

Fig. 4. Comparison between the experimental hardness profile obtained with nano-indentation: (a) nitrogen atoms distribution and (b) titanium atoms distribution measured by AES.

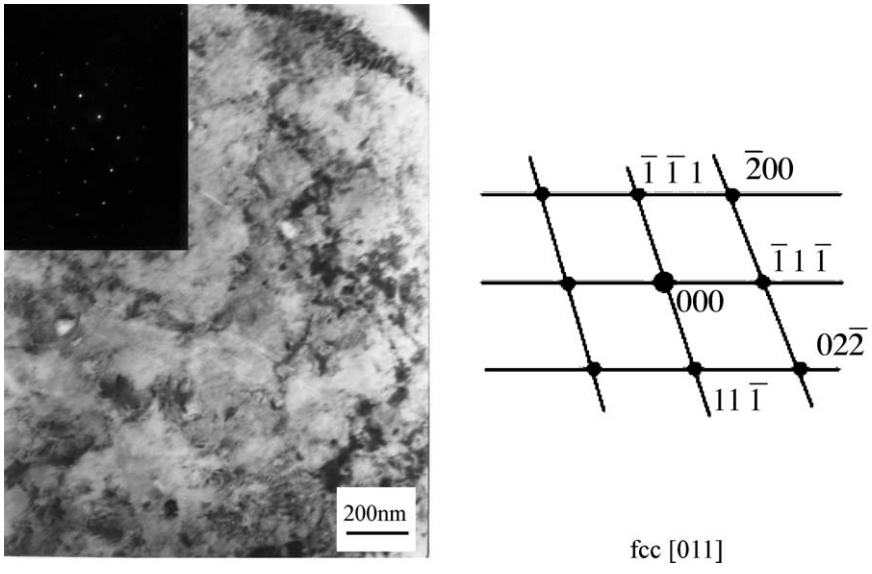

Fig. 3. TEM micrograph of the unimplanted substrate and its electron diffraction pattern.

the coefficient of sputtering, $S(\Phi)$ the diminished thickness of the surface after implanting a dose of Φ (nm), D the coefficient of diffusion corresponding to the Arrhenius equation ($\ln D - 1/T$), t the process duration (s), R_p the ion projected range, and ΔR_p is the straggle. Compared to Fe, N has a greater affinity with Cr, which is beneficial for nitrogen dissolution into the γ-Fe phase. It results in the apparent rise of the lattice parameters of the austenite phase producing the effects of solution strengthening. Meanwhile, chromium atoms and dislocations act as traps reducing the nitrogen atom mobility leading to the formation of a nitride layer (Cr_2N and CrN) around R_p [16]. The hardness of the N implanted layer is strongly related to the amount of N. It is most likely that the hardness profile of the N implanted sample is dominated by the synthetic effects of these two.

Different from nitrogen implantation, the Ti atoms display a typical Gaussian distribution in the substrate. The implantation temperature can be calculated between $0.25T_m$ and $0.6T_m$. In this case, thermal vacancies and recombination of vacancies and interstitial atoms can be neglected [31,32]. The densities of vacancies (C_v) and interstitials atoms (C_i) are directly proportional to the emergence efficiency which can be given as:

$$C_\nu = \frac{K_0}{D_\nu K_\nu^2} \tag{4}$$

and

$$C_i = \frac{K_0}{D_i K_i^2} \tag{5}$$

where K_i^2 and K_ν^2 represent the penetration intensity of interstitials atoms and vacancies, respectively, D_i^2 and D_ν^2 the diffusion coefficients, and K_0 expresses emergence efficiency of the two. C_v and C_i cause implanted Ti atoms to precipitate at the preferred sites full of defects leading to the formation of compounds and intermetallic phases. In agreement with the theoretical analysis, the strengthening phases of Ni_3Ti and $Ti_{5.73}C_{3.72}$ appear in the X-ray diffraction pattern. In addition, the heavier Ti ions result in more severe radiation damage and deformation of the shallower surface during the implantation process. It promotes the growth of the dispersion phases mainly at a shallower depth where it is full of dislocations and grain boundaries caused by radiation damage. Therefore, radiation damage plays an important role in the hardness improvement in the Ti implanted layer on 321 stainless steels. The larger the thickness of the Ti implanted layer or the broader the Ti distribution, the least is the enhancement effect. This is the reason why the location of the highest hardness of the Ti implanted layer displays a shift from R_p.

4. Conclusion

AES depth profiles show that the implanted titanium atoms are mainly distributed around the depth of 33 nm whereas the implanted nitrogen atoms display "as-implant" shape with the R_p of 77 nm. GIXRD patterns show that different strengthening phases are formed in the implanted layers. The nano-indentation test shows improved hardness for both the N and Ti implanted 321 stainless steel samples. The titanium implanted sample shows more strengthening at a shallower depth compared to the N implanted sample. It is because during implantation, the Ti ions cause more severe radiation damage and deformation of the surface than N ions. It not only creates dislocation strengthening, but also provides a large amount of defects where the intermetallics phases such as Ni_3Ti and compounds form and assemble contributing to the increased hardness. Hence, the hardness is mostly enhanced at a shallower depth, despite a shift from the R_p zone. With regard to the N implanted sample, the implanted layer is strengthened mainly by the formation of expanded austenite γ_N, namely solution strengthening. The improvement in the hardness is determined by the amount of N and since substantial diffusion has taken place, the maximum value of hardness is obtained at a larger depth at high nitrogen concentration (∼75 nm).

Acknowledgement

The work was financially sponsored by City University of Hong Kong, Direct Allocation Grant 9360110.

References

[1] N.E.W. Hartley, Wear 34 (1975) 427.
[2] G. Dearnaley, Thin Solid Films 107 (1983) 315.
[3] J.P. Riviere, P. Meheust, J.P. Villain, C. Templier, M. Cahoreau, G. Abrasonis, L. Pranevicius, Surf. Coat. Technol. 158–159 (2002) 99.
[4] G. Dearnaley, Nucl. Instrum. Methods B 50 (1990) 358.
[5] P. Sioshansi, Nucl. Instrum. Methods B 37–38 (1989) 667.
[6] O.K. Hubler, F.A. Smidt, Nucl. Instrum. Methods B 7–8 (1985) 151.
[7] K.K. Shih, Wear 105 (1985) 341.
[8] B. Rauschenbach, V. Heera, J. Less Common Met. 117 (1986) 323.
[9] R. Pratap, M.H.N. Beshai, R.T. Dhamejani, Thin Solid Films 146 (1987) L33.
[10] H.W. Wang, D.Z. Yang, W.D. Shi, S. Patu, Nucl. Instrum. Methods B 108 (1996) 371.
[11] R.R. Manory, C.L. Li, C. Fountzoulas, J.D. Demaree, J.K. Hirvonen, R. Nowak, Mater. Sci. Eng. A 253 (1998) 319.
[12] E. Richter, R. Günzel, S. Parasacandola, T. Telbizova, O. Kruse, W. Möller, Surf. Coat. Technol. 128–129 (2000) 21.
[13] W. Möller, S. Parasacandola, T. Telbizova, R. Günzel, E. Richter, Surf. Coat. Technol. 136 (2001) 73.
[14] A.V. Byeli, O.V. Lobodaeva, S.K. Shykh, V.A. Kukareko, Wear 181–183 (1995) 632.
[15] F.Z. Cui, H.D. Li, X.Z. Zhang, Nucl. Instrum. Methods 209–210 (1983) 881.
[16] H. Pelletier, P. Mile, A. Cornet, J.J. Grob, J.P. Stoquert, D. Muller, Nucl. Instrum. Methods B 148 (1999) 824.
[17] M. Iwaki, Mater. Sci. Eng. 69 (1985) 211.
[18] K. Saito, T. Matsushima, Mater. Sci. Eng. A 115 (1989) 355.
[19] G. Dearnaley, Mater. Sci. Eng. 69 (1985) 155.
[20] P.J. Evans, J. Hyvarinen, M. Samandi, Surf. Coat. Technol. 71 (1995) 151.
[21] G. Linker, Mater. Sci. Eng. 69 (1985) 105.
[22] S. Taniguchi, A. Kitahara, S. Wakayama, E. Eriguchi, N. Suyama, Nucl. Instrum. Methods B 175–177 (2001) 647.
[23] K. Sridharan, J.R. Conrad, F.J. Worzala, R.A. Dodd, Mater. Sci. Eng. A 128 (1990) 259.
[24] R. Saha, W.D. Nix, Mater. Sci. Eng. A 319–321 (2001) 898.
[25] W.C. Olivier, G.M. Pharr, J. Mater. Res. 7 (1992) 1564.
[26] T. Chudoba, N. Schwarzer, F. Richter, Thin Solid Films 355–356 (1999) 284.
[27] M. Göken, M. Kempf, W.D. Nix, Acta Mater. 49 (2001) 903.
[28] W.C. Oliver, G.M. Pharr, J. Mater. Res. 7 (1992) 1564.
[29] W.C. Oliver, G.M. Pharr, J. Mater. Res. 11 (1996) 760.

[30] K.S. Grabowski, R.A. Kant, in: H. Ryssel, Glawisching (Eds.), Ion Implantation Equipments and Techniques, Springer-Verlag, 1983, p. 364.
[31] T.H. Zhang, J.C. Zhou, J.H. Shen, J. Chen, J.H. Yang, Y.Z. Gao, G.R. Sun, F.J. Tan, J. Beijing Normal Univ. (Nat. Sci.) (Chin.) 4 (1990) 45.
[32] T.H. Zhang, C.Z. Ji, J.H. Shen, Nucl. Instrum. Methods 72 (1993) 409.
[33] D.L. Williamson, O. Ozturk, Nucl. Instrum. Methods B 59–60 (1991) 737.
[34] M.A. El Khalani, Nucl. Instrum. Methods B 59–60 (1991) 815.
[35] B. Bai, P.C. Zhang, J.S. Zou, Y.R. Chen, Acta Metall. Sin. (Chin.) 37 (2001) 82.